Tellus (2004), 56A, 472–484
Printed in UK. All rights reserved

TELLUS

Response of a global atmospheric forecast model to various drag parametrizations

By YOUNG-JOON KIM* and TIMOTHY F. HOGAN, *Naval Research Laboratory, Marine Meteorology Division, 7 Grace Hopper Ave, Stop 2, Monterey, CA 93943, USA*

(Manuscript received 4 December 2003; in final form 2 June 2004)

ABSTRACT

Various drag mechanisms are currently parametrized in numerical models of the atmosphere. For global models that include the middle atmosphere in particular, these mechanisms profoundly affect weather forecast as well as climate simulation. We have developed an extended-top version of the Navy Operational Global Atmospheric Prediction System (NOGAPS) to include the middle atmosphere by modifying some physical parametrizations and the vertical coordinate. We performed a series of ensemble simulations corresponding to January 2000 for investigating the response of the model to various drag mechanisms, such as mountain drag, orographic gravity wave drag, surface friction drag, and artificial model top drag. Based on the monthly mean fields obtained from the simulations, we first investigate the effect of gravity wave drag due to its direct impact through planetary wave activity as well as indirect impact through induced meridional circulation. We discuss the difficulties in partitioning between the mountain drag due to resolved orography and the gravity wave drag due to unresolved orography, first using conventional diagnostic measures. From analyses of the atmospheric angular momentum budget, we show that various model drag mechanisms when modified interact with one another by redistributing their drag while conserving the total amount. In particular, an overestimation of mountain drag is accompanied by an underestimation of gravity wave drag in the Northern Hemisphere mid-latitudes to conserve the total amount of drag in the model while likely breaking an optimal balance among the mechanisms. Under such a condition, the inclusion of a gravity wave drag parametrization – even if the drag amount itself is reasonable – does not necessarily improve the performance of the model. Diagnosis of this type of imbalance is not clear by conventional monthly mean fields of variables. In this paper, we argue that the budget of atmospheric angular momentum is a useful measure to diagnose impact of such changes in model physics with regard to the partition and balance among drag mechanisms. We also discuss the experimental results that led to the replacement of silhouette orography by mean orography in our model.

1. Introduction

The inclusion of the middle atmosphere allows for global atmospheric models to more realistically represent the feedback mechanisms between the upper and lower atmospheres. Among the important processes that should be represented in these models are drag/damping/dissipation mechanisms such as 'mountain drag' due to resolved mountains, 'gravity wave drag' (GWD) due to subgrid-scale mountains, artificially imposed 'model top damping' to suppress spurious reflection of waves, which contaminates numerical simulation, as well as 'friction drag' due to subgrid-scale turbulence in the planetary boundary layer. These drag mechanisms, except for friction drag, directly affect the magnitude of the polar night jet. Variations in the polar night jet can significantly modify the tropospheric circulation (e.g. Boville, 1984; Kodera et al., 1990; Kuroda, 2002) as well as the stratospheric circulation. Successful simulation of the polar night jet is therefore important in a global atmospheric model. The inclusion of these drag mechanisms in the model requires, however, careful representation of relevant physical processes owing to their significant indirect impact on the lower atmosphere (aka 'downward control'; Haynes et al., 1991) as well as their direct impact on the middle atmosphere.

Validation of any drag mechanism in a global atmospheric model is commonly performed by comparison with observations or analyses of first-order simulated fields such as the zonal wind, temperature, and sea level pressure, and also of derived fields such as the 'Eliassen–Palm (E–P) flux' (e.g. Andrews et al., 1987). Swinbank (1985) and Boer and Lazare (1988) performed refined studies to delineate model response to imposed drag mechanisms by analyzing the budget of the 'atmospheric angular momentum' (AAM). The AAM, which is exchanged between the atmosphere and the Earth, is a globally conserved

*Corresponding author.
e-mail: kimyj@nrlmry.navy.mil

quantity and thus its global imbalance in an atmospheric model can be expected to produce systematic errors in short-term forecasts and climate drift in long-term simulations (Huang et al., 1999). The fluctuation of the AAM also affects the length of day and is linked closely with atmospheric energy conversion processes and atmospheric variability. Bell et al. (1991) and Salstein et al. (1993) proposed the use of the AAM as a diagnostic quantity for testing global numerical weather prediction models.

Swinbank (1985) and Boer and Lazare (1988) compared the AAM calculated from analyses with the torques due to resolved mountain and parametrized surface friction. Boer (1990) included the gravity wave torque in the calculation of friction torque using analysis data, while Lejenäs et al. (1997) separately computed the gravity wave torque in addition to the mountain and friction torques using simulation data. These studies and also Klinker and Sardeshmukh (1992) imply that GWD is a possible source of bias in the vertically integrated AAM budget. Huang et al. (1999) found a large negative bias in the AAM due to GWD parametrization, which overcompensates the deficit of the AAM. Egger (2003) indeed stressed that GWD parametrization can be fraught with uncertainties. Given the uncertain role of the gravity wave torque, Huang et al. (1999) recommended a thorough investigation of the impact of GWD parametrizations on the variability of the AAM in global models.

In order to improve the range of forecast by properly representing the effects of the middle atmospheric physical processes such as the drag processes discussed above, we are gradually extending the top of the Navy Operational Global Atmospheric Prediction System (NOGAPS) to include the middle atmosphere. In this paper, as a first step we investigate the sensitivity of a prototype version of the model to selected parametrized subgrid-scale drag processes: specifically, GWD, surface friction drag, mountain drag, and artificial drag near the model top. We discuss the results from a series of ensemble simulations by comparing the results in terms of the redistribution of the AAM due to these drag mechanisms as well as of the zonal mean temperature, sea level pressure, eddy heat flux, and E–P flux.

In Section 2 we introduce the model used for this study including brief descriptions of the new GWD parametrization schemes and other relevant model physics investigated in this study. In Section 3, we describe the diagnostic measures used in this study including the AAM budget equations used for calculating the torques, which provides the basis for the design of our experiments described in Section 4. In Section 5 we present the experiment results along with discussions. A brief summary and remarks are given finally in Section 6.

2. Model description

NOGAPS is a global weather forecast/data assimilation system developed at the Naval Research Laboratory (NRL). The forecast component of NOGAPS is a global spectral model in the horizontal and energy-conserving finite difference model in the vertical. Details of the operational model can be found in Hogan and Rosmond (1991), Hogan et al. (1991), Rosmond (1992), and Hogan and Brody (1993). Major physical parametrizations are the bulk Richardson number dependent vertical mixing parametrization, surface flux parametrization (Louis 1979), shallow cumulus mixing parametrization, deep cumulus convection parametrization (Emanuel and Zivkovic-Rothman, 1999), convective and stratiform cloud parametrization (Slingo, 1987), subtropical boundary layer cloud parametrization (Teixeira and Hogan, 2002), solar and terrestrial radiation parametrization (Harshvardhan et al., 1987), orographic GWD parametrization (Palmer et al., 1986), and form drag parametrization through a systematic increase of the roughness over orography. The orographic roughness is enhanced by adding to surface roughness the values calculated from a formula similar to eq. (13) of Milton and Wilson (1996), but without the stability factor. The model orography is derived from the 2-min resolution National Imagery and Mapping Agency (NIMA) elevation data using a silhouette method that utilizes directionally dependent maximum peaks in each subgrid box. Newtonian cooling type of damping is semi-implicitly applied at the topmost two model levels to the equation for the virtual potential temperature whose vertical gradient is relaxed toward the isothermal condition. Its damping coefficient is defined as $K_c^{-1}[s] \propto M(M+1)/a^2$, where M is the number of waves (i.e. spectral resolution) and a is the radius of the Earth, so that the damping is selectively imposed on higher wavenumbers (Because of this scale-selective nature of our formulation, we refer to it as 'Newtonian damping' instead of 'Newtonian cooling'.)

To include the middle atmosphere, we developed a prototype research version of NOGAPS with an extended top, which is based mainly on the tropospheric operational version, but with upgrades in the GWD parametrizations and modifications in the treatments of long-wave radiation and mixing due to shallow cumulus. We replaced the orographic GWD parametrization scheme by the scheme of Kim and Arakawa (1995). This scheme takes into account 'selective enhancement' of low-level GWD due to resonant amplification of non-linear/non-hydrostatic gravity waves in downstream regions of subgrid-scale mountains, which was found beneficial in improving both climate simulations (Kim, 1996) and weather forecasts (Jordan Alpert, personal communication). We also coded and implemented the new convective GWD parametrization based on the formulations by Chun and Baik (1998). This parametrization treats cumulus clouds as 'obstacles' to the background wind for stationary heat sources, which distort the flow and generate 'convective' gravity waves, in a manner similar to that for orographic gravity waves (see also Chun et al., 2001). Moreover, we adjusted the long-wave radiation parametrization using a procedure similar to that of Kim et al. (1998) for better representing the CO_2 cooling rate near the model top, thereby alleviating a known deficiency in the scheme of Harshvardhan et al. (1987) in treating above 3 hPa as reported by Chou and Peng (1983). The depth of shallow cumulus mixing, which mixes the vertical potential temperature and

specific humidity, is constrained to a fixed value of 300 hPa for the maximum permitted pressure thickness measured from the surface to which shallow cumulus mixing can extend. A sigma-pressure hybrid vertical coordinate is used with the interface set at 100 hPa, instead of the pure sigma coordinate used in the operational version. The resolutions used in this study are T63 (=1.875°) and 36 levels with the top level at around 0.1 hPa (~60 km).

3. Diagnostic measures

3.1. Atmospheric angular momentum budget equation

As discussed in the introduction, the AAM is a useful quantity for investigating the impact of changes in drag mechanisms. The rate of change of the AAM plus the divergence of the meridional AAM transport should balance the sum of various torques due to the irregularity of the Earth's surface, e.g. the 'mountain torque' and the 'friction torque' (Swinbank, 1985; Boer and Lazare, 1988) as well as the 'gravity wave torque' due to subgrid-scale gravity waves (e.g. Huang et al., 1999). On vertically integrating and taking zonal and temporal averages, the following equation results (Swinbank, 1985; Boer and Lazare, 1988) with the terms we added due to gravity waves:

$$\frac{\partial}{\partial t}\left[\int_0^{p_s} m\frac{\mathrm{d}p}{g}\right] + \frac{1}{a\cos\varphi}\frac{\partial}{\partial\varphi}\left\{\left[\int_0^{p_s} mv\frac{\mathrm{d}p}{g}\right]\cos\varphi\right\} = -\left[\int_0^{p_s}\frac{\partial\Phi}{\partial\lambda}\frac{\mathrm{d}p}{g}\right] - a\cos\varphi\left\{[\tau_{\mathrm{Fr}}] + [\tau_{\mathrm{GW}}]\right\}. \quad (1)$$

Here, t is time, m ($\equiv \Omega\, a^2\cos^2\varphi + ua\cos\varphi$) is the (absolute) AAM per unit mass, Ω is the angular velocity of the Earth's rotation, φ is the latitude, u and v denote, respectively, the zonal and meridional winds, p is the atmospheric pressure, g is the gravity, Φ is the geopotential, λ is the longitude, and τ_{Fr} and τ_{GW} are the zonal stresses due, respectively, to surface friction and subgrid-scale GWD. The subscript 's' denotes surface values and the square bracket represents the zonal average.

We can neglect the first term on the left-hand side of eq. (1) based on the assumption that the monthly local tendency of integrated and averaged m can be neglected. By evaluating each term on the right-hand side (representing mountain torque, friction torque, and gravity wave torque from left to right) and comparing their sum with the second term of the left-hand side, we can check the adequacy of the collective monthly magnitude of the right-hand side terms represented in the model. This equation forms the main basis for the design of our experiments, which is discussed in Section 4.

3.2. Residual mean stream function

The time-averaged residual mean meridional circulation approximates the mean motion of air parcels and thus the mean advective transport of the trace substances. The 'residual mean stream function' (Peixoto and Oort, 1992) based on the transformed Eulerian-mean framework (Andrews et al., 1987) can be written as

$$\tilde{\psi} = \frac{2\pi a\cos\varphi}{g}\left\{\int_0^p [v]\mathrm{d}p - [v^*\theta^*]/\frac{\partial\theta_{\mathrm{o}}}{\partial p}\right\}\Big/\rho_{\mathrm{o}}, \quad (2)$$

where π is the ratio of the circumference of a circle to its diameter, θ is the potential temperature, ρ is the atmospheric density. Here, the subscript 'o' denotes the average on a given pressure level and the asterisk represents deviation from the zonal average. We divide the stream function by ρ_{o} for greater visibility of stratospheric values as included in eq. (2).

3.3. Eliassen–Palm flux and divergence

The E–P flux based on the transformed Eulerian mean zonal momentum framework provides useful diagnostics for understanding the interaction between zonally asymmetric disturbances and the zonal mean circulation (Edmon et al., 1980). The net eddy forcing can be efficiently represented by the divergence of the E–P flux (Andrews and McIntyre, 1976; Boyd, 1976). We express the E–P flux vector ($\boldsymbol{F}$) and its divergence as

$$F^{\varphi} = -\rho_{\mathrm{o}} a\cos\varphi[u^*v^*]/\rho_{\mathrm{o}}$$

$$F^{p} = \rho_{\mathrm{o}} f a\cos\varphi[v^*\theta^*]\left(\frac{\partial\theta_{\mathrm{o}}}{\partial p}\right)^{-1} R/\rho_{\mathrm{o}}$$

$$\nabla\cdot\boldsymbol{F} = \left\{\frac{1}{a\cos\varphi}\frac{\partial}{\partial\varphi}(F^{\varphi}\cos\varphi) + \frac{\partial}{\partial p}F^{p}\right\}\Big/(\rho_{\mathrm{o}} a\cos\varphi), \quad (3)$$

where f is the Coriolis parameter. For graphical clarity at upper part of the model domain while preserving the physical meaning, we divide the horizontal and vertical vector components and divergence, respectively, by ρ_{o}, ρ_{o}/R and $\rho_{\mathrm{o}} a\cos\varphi$ as applied to eq. (3), where R is the ratio of the horizontal to vertical plot domain length. We choose this quasi-geostrophic form not only for its simplicity but also because of the unavailability of reliable vertical (pressure) velocity from our analysis used for comparison, which is necessary to compute a more general E–P flux vector based on primitive equations (Andrews et al., 1987). Although a straightforward interpretation of the quasi-geostrophic E–P flux divergence as a diagnostic of the wave-mean flow interactions in the stratosphere may not always be possible (see Robinson, 1986), it provides us with a basic measure of planetary wave driving that is not available from the mean variables.

4. Experimental design

We designed sensitivity experiments based on the arguments pertaining to eq. (1) on the balance among the drag due to gravity waves, surface roughness and resolved orography, and also on damping near the model top (Table 1). The control experiment (CTRL) includes all the components of the modified physics

Table 1. Sensitivity experiments performed with an extended-top version of NOGAPS, designed by excluding orographic GWD (NoOG), Newtonian damping (NoND), form drag (NoFD) all using the NIMA orography, and by using the previous version of resolved orography derived from the US Navy terrain data (XORO). Also performed is without using the silhouette enhancement for the NIMA orography, i.e. using mean orography (MORO).

Experiment	CTRL	NoOG	NoND	NoFD	XORO	MORO
Orographic GWD	Yes	No	Yes	Yes	Yes	Yes
Newtonian damping	Yes	Yes	No	Yes	Yes	Yes
Enhanced surface roughness	Yes	Yes	Yes	No	Yes	Yes
Resolved orography	NIMA Silhouette	NIMA Silhouette	NIMA Silhouette	NIMA Silhouette	US Navy Silhouette	NIMA Mean

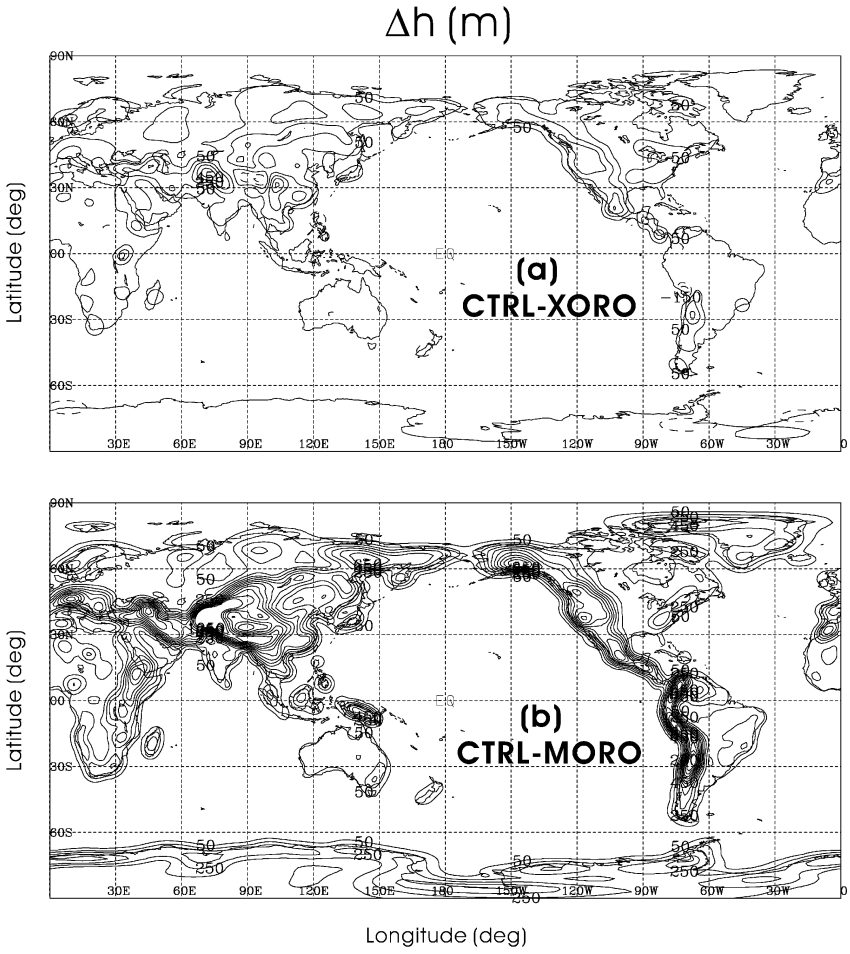

Fig 1. The difference in height (m) of the control (CTRL) silhouette orography from (a) the previous (XORO) silhouette orography and (b) the mean (MORO) orography, for T63 resolution used in NOGAPS. The control silhouette orography and the mean orography are derived from the 2-min terrain data by NIMA and the previous silhouette orography is from the 10-min US Navy terrain data.

and uses the NIMA silhouette orography. Experiment NoOG is without the orographic GWD parametrization, NoND is without Newtonian damping, NoFD is without the 'form drag' (i.e. no enhancement of the surface roughness parameter). (We do not discuss the impact of the convective GWD in this study for the reason given in Section 5.2.) Experiment XORO is with the previous version of silhouette orography used for NOGAPS derived from the 10-min US Navy data while MORO is with the NIMA mean orography to be discussed in later part of this study.

The difference between the control (NIMA silhouette) orography and the Navy silhouette orography is shown with respect to T63 (=1.875°) resolution in Fig. 1a. The control silhouette orography is overall significantly higher than the Navy silhouette orography.

We perform sensitivity simulations with the model without involving data assimilation as the first step, as done by, for example, Milton and Wilson (1996). This has its own merit because a data assimilation procedure can mask systematic errors of a forecast

model although it improves the forecast. We initialize the model with the NRL's 'Multi-Variate Optimal Interpolation' (MVOI; Barker, 1992; Goerss and Phoebus, 1992) analysis at 00 UTC on 20 December 1999. We generate two perturbations to the original initial conditions by running 24- and 48-h simulations and also obtain two additional perturbations by running the normal mode initialization procedure again on these simulations, thereby generating a five-member ensemble for each experiment. We have found this procedure is statistically very similar to starting the model from various dates around 20 December 1999. For identifying long-term systematic model errors, we integrate the model for 41 d through the end of January 2000 and average the last 31 d of the simulations to generate the January 2000 mean. To check the statistical validity of the difference among these sensitivity experiments, we first compared standard deviations of the ensembles of the temperature, zonal winds and sea level pressure for each experiment with those among the experiments and confirmed that the variations within the ensemble members of each experiment are smaller than those between the experiments. We also performed the standard student *t*-test and confirmed that the differences among the experiments have high statistical significance, particularly in the northern polar stratosphere (an example is shown in the next section).

5. Results and discussion

We present here the results from the ensemble of sensitivity simulations for January 2000. We look into the monthly mean zonal mean fields of selected model variables and vertically integrated momentum torques. We compare the response of the model to the changes in drag mechanisms listed in Table 1.

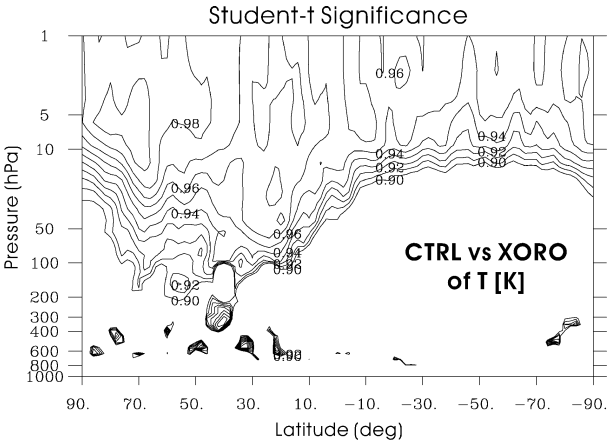

Fig 3. As in Fig. 2d, but for the student *t* significance of the temperature (K) between CTRL and XORO. The contours are shown for 0.9 (90%) or higher.

5.1. Impact on the mean flow and waves

Figure 2 compares the sensitivity of the simulated zonal mean temperature to the omission of various drag mechanisms. When orographic GWD is excluded (NoOG) or previous orography is used (XORO), significantly warmer polar stratosphere than CTRL is simulated. The statistical significance of this temperature difference from CTRL in terms of the student *t* statistics is given in Fig. 3; shown is for XORO that involves the largest temperature difference (Fig. 2d). The region of the maximum difference overlaps well with high significance values.

The tendency of the zonal mean wind due to orographic GWD obtained from CTRL experiment is shown in Fig. 4. The

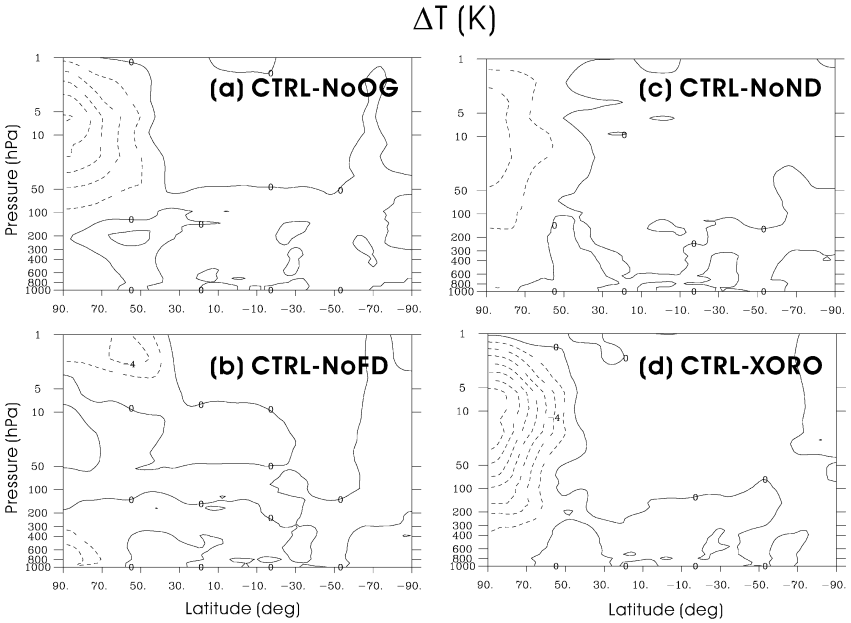

Fig 2. The difference in the zonal mean temperature (K) simulated by NOGAPS T63L36 between the CTRL simulation and the simulations performed without (a) orographic GWD, (b) form drag, (c) Newtonian damping, and (d) the simulation performed with previous orography derived from the US Navy data. Each simulation is the average of five-member ensemble experiments. Contour interval is 2.

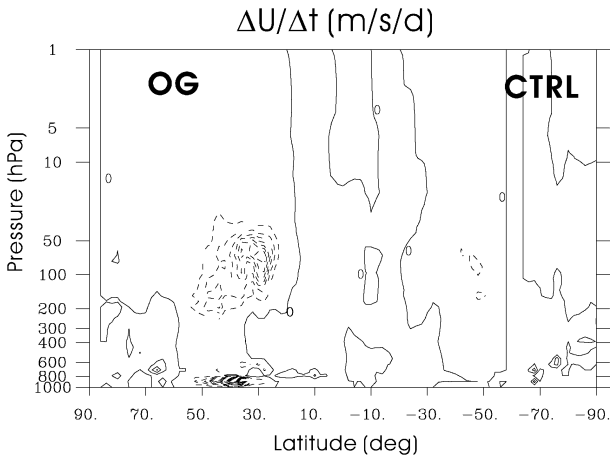

Fig 4. The tendency of the zonal mean zonal wind (m/s/d) due to orographic GWD, obtained from the NOGAPS T63L36 control simulation for January 2000. Contour interval is 0.25.

orographic GWD generates large westward drag near the surface and around 100 hPa over mid-latitude mountainous regions in the Northern Hemisphere. The small magnitude of GWD at upper levels is by an ad hoc density factor (the ratio of density values at two adjacent levels) multiplied to GWD to avoid the model's tendency to degrade the forecast skill near the surface with strong GWD at upper levels. It is interesting that the presence of the GWD cools most of the northern polar lower stratosphere (Fig. 2a). According to the conventional impact of northern mid-latitude GWD near the model top on the simulated atmosphere as shown by Palmer et al. (1986) and illustrated by Kim et al. (2003), the presence of such drag usually involves warming below and poleward of the region of drag maximum. This is because of the secondary meridional circulation induced by GWD. Unlike such a situation in which the drag maximum is located near the model top, our maximum drag is located in the middle of the vertical domain around 100 hPa (Fig. 4). As described by Milton and Wilson (1996), a clockwise indirect meridional circulation above the orographic GWD maximum can be forced as well as a counterclockwise indirect circulation below it. The upper branch of the circulation induced by GWD then involves poleward and upward motion near the North Pole, which leads to adiabatic cooling above the maximum GWD level, while the impact of the downward motion is also seen as warming in the troposphere in the northern high latitudes (Fig. 2a) and also increases in the northern high-latitude pressure (Fig. 5). Overall, the upward motion dominates the impact of GWD on the temperature. This 'dipole pattern' of the temperature difference field resembles the 'quadruple pattern' response to GWD reported by Shepherd et al. (1996, their fig. 6) and McFarlane (1987, his fig. 13).

We now try to verify this interpretation in terms of the residual mean stream function, defined by eq. (2). Figure 6 shows the difference of $\bar{\Psi}$ between CTRL and NoOG. In the Northern Hemisphere, this difference field shows the clockwise/counterclockwise circulation due to orographic GWD in the stratosphere/troposphere, which induces cooling/warming in the northern polar stratosphere/troposphere as shown in Fig. 2a. This dipole structure of the induced circulation is closely linked to the location of the maximum drag, which is around 100 hPa (Fig. 4), implying that the details of the GWD parametrization can significantly alter the structure of the meridional circulation. Our thermal and residual circulation responses to this winter GWD forcing are just what might be expected for the relatively short-term response to a momentum forcing, following Haynes et al. (1991) on 'downward control' as discussed by Shepherd et al. (1996). However, the secondary circulation does not seem sufficient to explain the temperature difference between CTRL and NoOG (Fig. 2a) because the secondary circulation is not strong directly over the northern polar stratosphere (Fig. 6) where the maximum temperature difference exists. Then, the temperature change by the GWD process may also be due to an associated change in the planetary wave activity through a

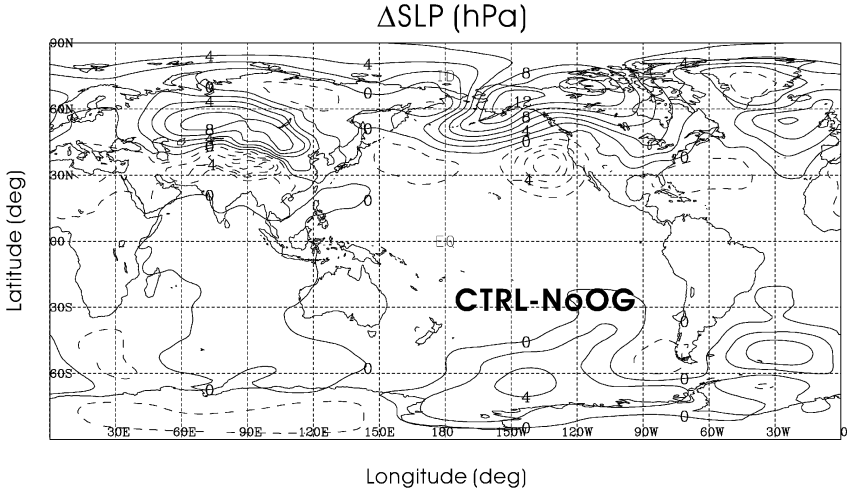

Fig 5. As in Fig. 2a, but for the sea level pressure (hPa).

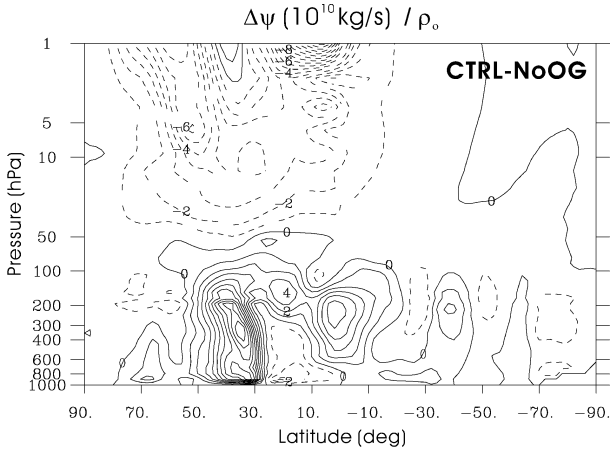

Fig 6. As in Fig. 2a, but for the residual mean stream function (10^{10} kg s^{-1}). The contour values have been scaled by the density for graphical clarity. Negative (dashed) and positive (solid) contours denote, respectively, clockwise and counterclockwise residual circulations.

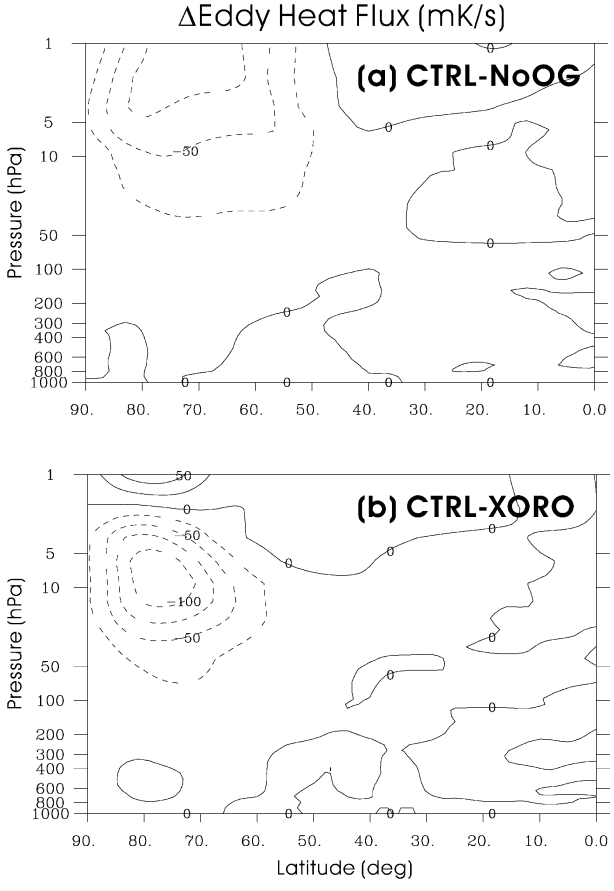

Fig 7. As in Figs. 2a and 2d, but of the meridional eddy heat flux (mK s^{-1}) in the Northern Hemisphere. Contour interval is 25.

change in the mountain drag. This is indeed observed over polar stratosphere as the change in the stationary eddy heat flux field (Fig. 7a) that quantifies vertical propagation of planetary waves.

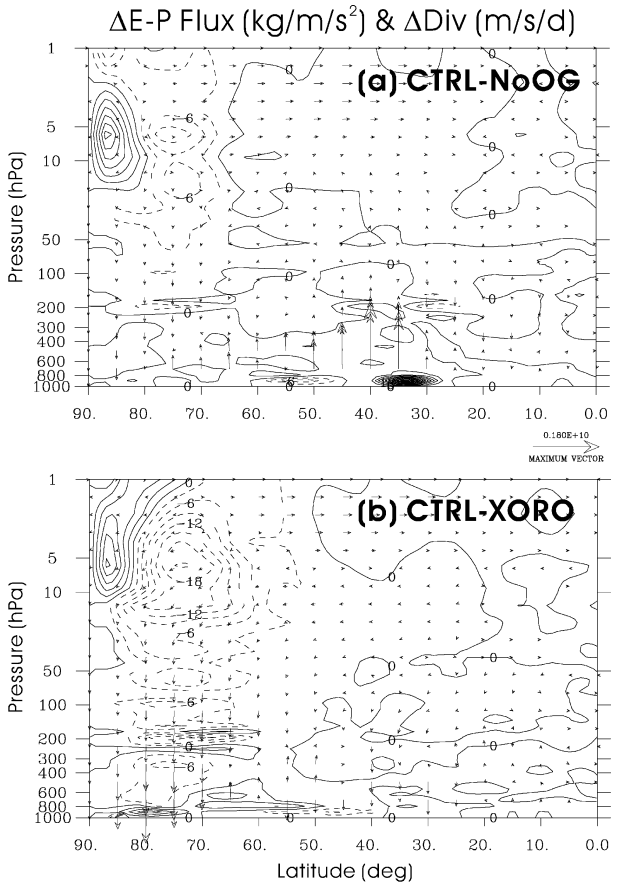

Fig 8. As in Fig. 7, but of the E–P flux (kg m^{-1} s^{-2}; vectors) and its divergence (ms^{-1} d^{-1}; contours).

It is worth noting that the use of the Navy orography also results in significantly warmer northern polar stratosphere (Fig. 2d). Because this sensitivity involves the effects of resolved orography, it is believed that the difference in mountain drag due to the differences in orographic heights played a role in such a way that the Navy orography (XORO) continually forces stronger planetary wave driving at upper levels. The zonal winds corresponding to the NoOG and XORO cases (not shown) reveal that the exclusion of GWD and the use of the Navy orography resulted in the largest weakening of the polar night jet, which is consistent with the largest differences in the temperature fields according to the thermal wind balance (Figs. 2a and 2d). To confirm this result, we calculate the E–P flux defined by eq. (3). Figure 8 compares the differences in the stationary E–P flux and its divergence of NoOG and XORO from CTRL, showing components of the wave-mean flow interaction due to GWD and the presence of enhanced orography. These two cases involve the largest differences from CTRL due to the changed sign of the divergences resulting in strong meridional gradients of the divergences in the northern polar stratosphere. This implies that in these experiments the wave-mean flow interaction is most active

and so is the planetary wave driving in the model. As is also confirmed by the eddy heat flux differences (Fig. 7), the impact of the GWD and increased resolved mountain on the model is similar, at least in the northern high latitudes. It is interesting to find that the stationary component of the planetary wave activity is greater in both NoOG and XORO, in that unlike the conventional result the planetary waves are reduced in our model by GWD and higher orography (see also Fig. 1).

5.2. *Impact on the atmospheric angular momentum budget*

We discussed in the introduction the importance of the AAM budget as a diagnostic measure for checking model response to changes in drag mechanisms. We now investigate the budget of the AAM in the model. Swinbank (1985) earlier inferred the meridional momentum flux divergence, i.e. the second term on the left-hand side of eq. (1), from January 1979 First Global Atmospheric Research Program (GARP) Global Experiment (FGGE) IIIa data for 2° latitude bands (his fig. 7), which is comparable to our model resolution of T63 (=1.875°). He used the inferred torque to validate the mountain and friction torques calculated from his model simulation, i.e. the first two terms on the right-hand side of eq. (1). The Swinbank's model-simulated torques (not shown) are in qualitative agreement with ours, although there are significant quantitative differences, which are considered to be due partly to the fact that gravity wave torque was not included in Swinbank's calculations. We use the torque inferred from the momentum flux divergence using the FGGE data for checking our values.

The total and individual components of the zonally averaged and vertically integrated torque calculated from the CTRL experiment are shown in Fig. 9a along with Swinbank's inferred torque obtained from the FGGE data. There are some discrepancies in the peak latitudes between the inferred torque and our total torque, especially in the Northern Hemisphere. The total

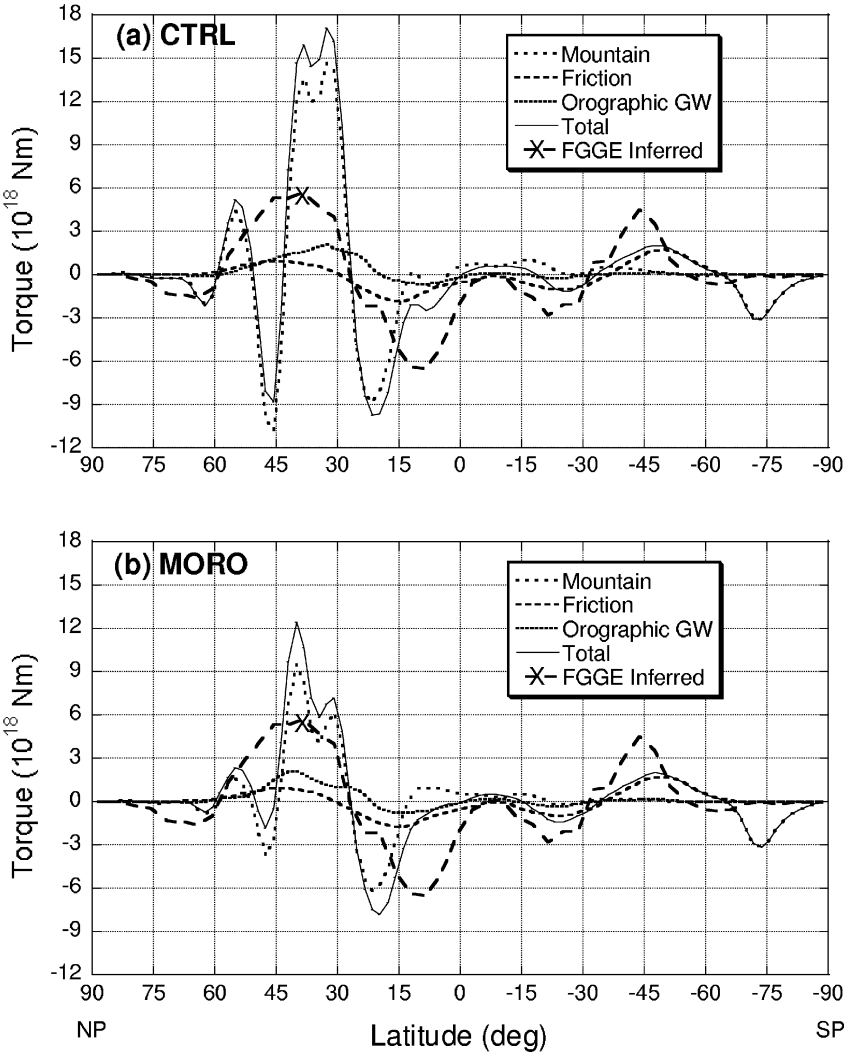

Fig 9. The zonally and vertically averaged torques (10^{18} Nm) for January 2000 simulated by NOGAPS T63L36 from the (a) CTRL (silhouette orography) and (b) MORO (mean orography) experiments. The torque inferred by Swinbank (1985) from the FGGE IIIa observation data is also plotted with its maximum value marked by 'X'.

torque is underestimated in the Southern Hemisphere (regardless of the orography used, as will be shown later). Therefore, assuming that the FGGE result is reasonably accurate (note that the FGGE is for January 1979 while ours is for January 2000), there is some fundamental deficiency in the model that underestimates the torque in the Southern Hemisphere. The most striking difference is, however, that our maximum simulated total torque is much larger than that of the inferred torque in the northern mid-latitudes (marked by 'X' in Fig. 9). This is mainly due to our overestimated mountain torque, which alone is about two times larger than that of the inferred torque. (The reason for this discrepancy will be discussed later in this subsection.)

We also investigate the impact of orographic GWD in view of the difference in the torque from the control experiment. The difference due to the GWD is the largest over the northern mid-latitudes, as expected (Fig. 10a). We note here that other torque terms also change significantly in response to the omission of orographic GWD; especially the mountain torque, which seems to try to balance the gravity wave torque of opposite sign in the northern mid-latitudes. This result demonstrates that the magnitudes of drag mechanisms in the model are determined not only by the individual parametrizations but also by their balance with other mechanisms, thus advising caution in the interpretation of an addition or removal of any drag mechanism in the model. Boer and Lazare (1988) reported that when GWD parametrization was removed in their model the surface torque was unexpectedly increased, interpreting their results as 'paradoxical' because they expected a decrease of surface torque. However, their results can be understood in terms of the angular momentum balance discussed in our study. When GWD is removed, the model tries to maintain the total amount of the drag by increasing the magnitude of other drag mechanisms. If GWD were considered in their budget, therefore, their results would have not been considered paradoxical but in fact quite expected. This issue is further related to the discussion of Egger (2003) that the impact of GWD should not be seen only in terms of wind deceleration, and that the response of the large-scale flow to gravity wave torque can also be understood in terms of a geostrophic adjustment process within the framework of global AAM conservation. Furthermore, we would like to note here that we implemented the convective GWD parametrization into the model without including the 'compensating acceleration' at cloud top needed to conserve the momentum due to convective GWD in a model column. We thus did not discuss its impact in this study, although this omission has relatively minor impact in our monthly simulations according to our tests. The convective GWD in our model plays a role smaller than but similar to the orographic GWD in that mountain torque is balanced by convective gravity wave torque in the northern mid-latitudes for January 2000.

The impact on the torques of the form drag parametrization implemented through systematic enhancement of the roughness length is shown in Fig. 10b. The surface drag enhancement does not change considerably the balance of the momentum compared with GWD although it is still non-negligible. This may look rather surprising considering the extent of the enhancement in the surface roughness, which is as large as 99 m, but is understandable in that the effect of form drag is mostly confined near the surface and suppressed by the stronger static stability in the northern winter.

The impact of Newtonian damping is shown in Fig. 10c. In the Northern Hemisphere, the torque is almost uniformly greater in NoND, which means that the AAM is systematically lost by the damping, resulting in an imbalance in the AAM redistribution. In principle, the positive and negative differences of the AAM should approximately be in global balance (i.e. zero sum) as roughly shown in other sensitivity experiments presented in Fig. 10. Again, the AAM redistribution due to any change in

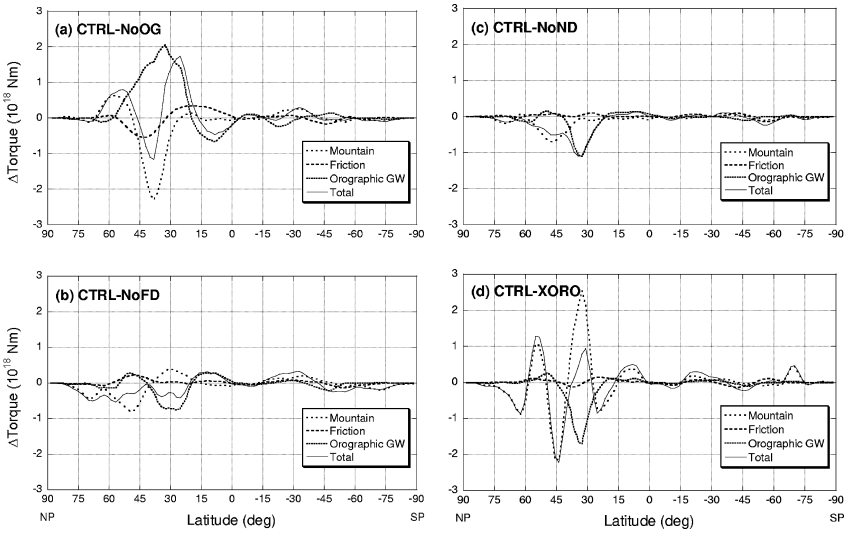

Fig 10. As in Fig. 9, but for the difference as in Fig. 2 and without the inferred torque.

drag is made while conserving the total amount (the global average should be zero in a perfect model). As we discussed in the introduction, several studies (e.g. Boer, 1990; Klinker and Sardeshmukh, 1992; Lejenäs et al., 1997; Huang et al., 1999) suspected GWD as a source of bias in the vertically averaged AAM budget. In our case as well, the GWD introduces bias in the angular momentum budget, which is latitude-dependent, but the Newtonian damping generates bias more systematic than that of GWD. This is likely to be due to its scale-dependent damping nature as described in Section 2, but may also be due to the lack of a constraint that the net drag over the sphere on a given level must vanish, as discussed by Shepherd et al. (1996).

The impact of the change in the resolved orography on the angular momentum budget is also as large as that of the CTRL–NoOG case (Fig. 10d). The mountain torque is significantly different between the two experiments over the northern mid-latitudes (with different signs depending on the signs of the orographic slopes and the winds). As expected from the results of CTRL–NoOG (Fig. 10a), subgrid-scale orographic gravity wave torque also responds strongly to this change in resolved-scale orographic height (through the direct changes in the wind speed and stability, associated with elevated or lowered surface of orography, which force gravity wave and their effects). It is clear that mountain torque and gravity wave torque strongly influence each other. These results confirm the fact that a change in drag through one drag mechanism is balanced by a compensating change through another drag mechanism to maintain the overall balance of the momentum budget, although the process is complex involving significant latitudinal variation.

Partitioning the parametrizations of the effects of subgrid-scale gravity waves through GWD and resolved planetary waves through mountain drag that is increased by enhanced orography such as envelope or silhouette orography has been a subject of debate since the introduction of the GWD parametrization in the 1980s, although the enhanced orography technique is now less favored especially with enhanced model resolutions (some thoughts on this issue are given in Kim et al., 2003). A comparison of the E–P flux vector differences (Fig. 8) reveals that the directions of the flux vectors and divergences for NoOG and XORO are qualitatively similar in the northern high-latitude stratosphere although XORO induces stronger vertical vectors and divergences. Thus, the impacts of orographic GWD and mountain drag in the northern high-latitude stratosphere are similar in view of both a derived field (the E–P flux) and a first-order field (the temperature) (Figs. 2a and 2d). This implies that it is particularly difficult to properly partition between the effects of parametrized drag (GWD) and resolved drag (mountain drag).

Furthermore, in order to investigate how a systematic difference in resolved orographic height affects the magnitude of mountain torque, we have performed an additional set of ensemble simulations with the 'mean orography' (MORO) derived from the NIMA data without using the enhancement algorithm for the silhouette orography. The difference between the silhouette orography and the mean orography is shown in Fig. 1b. The difference is an order of magnitude larger than that between the two silhouette orographic data sets (i.e. NIMA and Navy) shown in Fig. 1a. The impact on the torque (Fig. 9b in comparison with Fig. 9a) shows significantly reduced mountain torque and thus total torque. The torque is virtually unchanged in the Southern Hemisphere, which is due to the scarcity of major mountains and lower static stability in that hemisphere in January. The maximum total torque in the Northern Hemisphere is still excessive, but is much closer to that of the inferred torque based on the FGGE data (marked by 'X' in the figure). We conclude, therefore, that the magnitude of the total drag with the silhouette orography in our model is already too large even without GWD, and thus an addition of GWD results in degradation of the forecast through undesirable redistribution of the total drag. This degradation due to overestimated total drag is likely to be one of the main reasons why our operational NOGAPS with silhouette orography tends to degrade in the weather forecast skill by upper-level GWD.

5.3. *Impact on the forecast skill*

In order to see if the use of the mean orography actually leads to an improvement of the forecast skill compared with the silhouette orography based on NIMA or US Navy data, we performed the standard data assimilation/forecast experiments with NOGAPS. The forecast is performed with 6-h assimilation cycles consisting of the data quality control, tropical cyclone bogusing, the NOGAPS operational moisture analysis and optimum interpolation of winds and heights, sea-surface temperature and sea-ice concentrations from the US Navy analyses, and snow amounts from the US Air Force analyses. 5-d forecasts are run once a day from the 00 UTC initial conditions. Standard statistical scores, including mean errors, root mean square errors, and anomaly correlations (ACs) as defined in Rosmond (1992) are computed for each data assimilation/forecast integration run.

We used a lower-resolution version (T79L24 with its top at around 1 hPa or 40 km) of the operational model (T239L30), which has a lower top than the extended-top version due mainly to the limit in the vertical range of our data assimilation system. We performed three experiments using the NIMA silhouette orography (CTRL), the NIMA mean orography (CTRLm) and the US Navy silhouette orography (XORO). These experiments include all the components of the modified physics used for the sensitivity experiments listed in Table 1. As an example, Fig. 11 shows the 500-hPa geopotential height AC in the tropics for January 2000 (composed from the last 31 daily forecasts that started from 27 December 1999 and continued until the end of January 2000). As anticipated from the results of the torque analyses (Fig. 9), the forecast skill is superior with the use of the mean orography. Although these results are from a lower-top version of the model, they are consistent with the sensitivity experiment results and highlight the importance of the

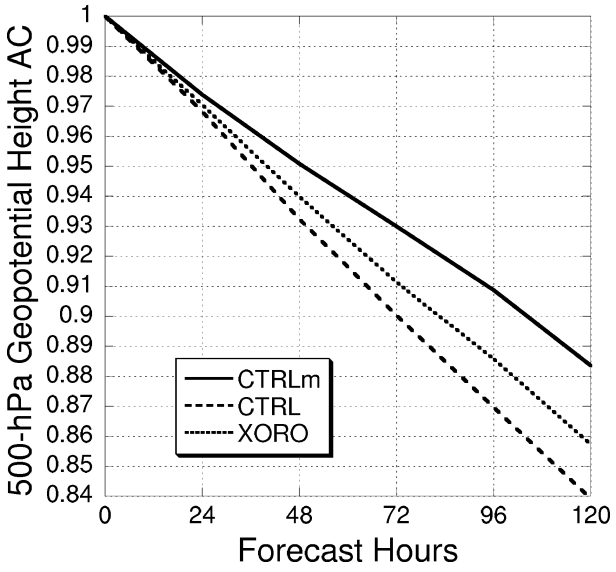

Fig 11. The anomaly correlations of the 500-hPa geopotential height (m) in the tropics (between 20°N and 20°S) for January 2000 for forecast/data assimilation experiments performed with a lower resolution version (T79L24) of the operational NOGAPS and the modified physics introduced in the present study. CTRLm, CTRL, and XORO denote the forecasts made with the NIMA mean orography, the NIMA silhouette orography and the US Navy silhouette orography, respectively.

effort to properly represent resolved model orography, which in practice should precede that for model physics improvement, particularly of GWD parametrization. Based on this and further studies, a version of the mean orography went operational into NOGAPS in November 2003.

6. Summary and remarks

In this study, we introduced a prototype extended-top version of the NOGAPS forecast model with resolution of T63L36 (top at around 0.1 hPa) and investigated its sensitivity to various drag parametrization mechanisms. A series of ensemble sensitivity simulations was performed for January 2000 and the response of the model to orographic GWD, mountain drag, form drag via enhanced roughness parameter, and artificial model top damping was discussed. The vertical distribution of our orographic GWD partially determined the impact of GWD in such a way that the northern polar stratosphere is cooled while the sea level pressure is increased in northern polar regions, respectively, by the upper and lower branches of the induced mean meridional circulation. The impact of GWD also involved a change in the magnitude of the planetary wave driving, contributing in fact more to the change in the temperature in the northern polar stratosphere, which is qualitatively similar to that of a change in resolved orography. The impacts of the form drag and Newtonian damping were not significant in view of the monthly means of basic model variables. The use of our previous version of the orography based on US Navy data produced the largest difference from the control in the response, which we understand as a realization of more active wave-mean flow interaction.

We showed that conventional diagnostics, such as the mean temperature and eddy fluxes, do not clearly identify the impact of drag processes, especially between GWD and mountain drag. We thus analyzed the balance among the drag mechanisms in view of the AAM budget by calculating the zonally averaged and vertically integrated torques due to the drag parametrizations. The results from the budget analyses demonstrate that the drag mechanisms interact with one another modifying the magnitude of each mechanism while conserving the total drag. For example, an omission of orographic GWD leads to an overall increase of mountain drag and vice versa, to compensate for the change while trying to conserve the amount of the total drag but likely breaking an optimal balance among the mechanisms. The sensitivities of the model to the form drag and Newtonian damping are relatively small as seen from the mean fields, but the Newtonian damping is shown to introduce a clear bias in the AAM budget. The results presented in this study illustrate the importance of the balance among drag parametrizations in global atmospheric models and recommend careful analysis and interpretation while adding or removing such a mechanism. Similar results have also been reported with higher resolution numerical weather prediction models (e.g. Rontu and Boutier, 2002; Rontu et al., 2002).

The present study, however, does not present any direct method to quantitatively validate individual drag mechanisms, although we can use the torque inferred from observation data in validating the total torque simulated by the model. A well-known approach is to validate parametrizations with respect to single columns of the model, on-line or off-line, using observation and/or simulation data. We are following this approach for further validating the GWD parametrizations with the aid of explicitly simulated high-resolution model data (as earlier done, for example, by Kim and Arakawa, 1995; Broad, 1996; Gregory et al., 1998).

The parametrization of GWD and the introduction of enhanced orography, such as envelope and silhouette, have become popular in many global atmospheric models as effective means to alleviate systematic model errors and improve simulation and forecast. The parametrization may improve the model systematic bias for the wrong reason, i.e. systematic errors could have been concealed by fortuitous rebalancing among the drag mechanisms, especially between GWD and mountain drag, which is closely related to the issue of the partition between them. As the models progressively become more sophisticated and adopt higher resolutions to resolve more explicit subgrid-scale processes, further validation of the models by additional measures, such as the AAM budget, may be useful.

The present study also shows that the use of mean orography instead of silhouette orography improves the budget of the AAM and the forecast skill in NOGAPS. It is, in fact, a

general trend in the modeling community that mean orography is favored over enhanced orography involving, e.g. an undesirable rejection of valuable data near the surface in data assimilation and an unrealistic enhancement of orographic rainfall (Lott and Miller, 1997), which becomes more serious as the resolution increases. This trend is especially true with the introduction of more physical representation of subgrid-scale low-level flow-blocking parametrizations (Lott and Miller, 1997; Scinocca and McFarlane, 2000), which we are in the process of including in the model (Kim and Doyle, personal communication).

7. Acknowledgments

The authors would like to thank Drs Stephen Eckermann, Larry Coy, John McCormack, Hye-Yeong Chun, Tom Rosmond, and Chi-Sann Liou for discussions and/or comments on the original manuscript, and the anonymous reviewers for useful suggestions and comments that improved the manuscript. They gratefully acknowledge the support from the sponsor, the Office of Naval Research under ONR Program Element 0602435N.

References

Andrews, D. G., Holton, J. R. and Leovy, C. B. 1987. *Middle Atmospheric Dynamics*. Academic, New York, 489 pp.

Andrews, D. G. and McIntyre, M. E. 1976. Planetary waves in horizontal and vertical shear: The generalized Eliassen–Palm relation and the mean zonal acceleration. *J. Atmos. Sci.* **33**, 2031–2048.

Barker, E. 1992. Design of the Navy's multivariate optimum interpolation analysis system. *Wea. Forecasting* **7**, 220–231.

Bell, M. J., Hide, R. and Sakellarides, G. 1991. Atmospheric angular momentum forecasts as novel tests of global numerical weather prediction models. *Phil. Trans. R. Soc. London A* **334**, 55–92.

Boer, G. J. 1990. Earth–atmosphere exchange of angular momentum simulated in a general circulation model and implications for the length of day. *J. Geophys. Res.* **95**, 5511–5531.

Boer, G. J. and Lazare, M. 1988. Some results concerning the effect of horizontal resolution and gravity-wave drag on simulated climate. *J. Climate* **1**, 789–806.

Boville, B. A. 1984. The influence of the polar night jet on the tropospheric circulation in a GCM. *J. Atmos. Sci.* **41**, 1132–1142.

Boyd, J. 1976. The non-interaction of waves with the zonally averaged flow on a spherical earth and the interrelationships of eddy fluxes of energy, heat and momentum. *J. Atmos. Sci.* **33**, 2285–2291.

Broad, A. S. 1996. High-resolution numerical-model integrations to validate gravity-wave-drag parametrization schemes: a case study. *Q. J. R. Meteorol. Soc.* **122**, 1625–1653.

Chou, M.-D. and Peng, L. 1983. A parametrization of the absorption in the 15 mm CO_2 spectral region with application to climate sensitivity studies. *J. Atmos. Sci.* **40**, 2183–2192.

Chun, H.-Y. and Baik, J.-J. 1998. Momentum flux by thermally induced internal gravity waves and its approximation for large-scale models. *J. Atmos. Sci.* **55**, 3299–3310.

Chun, H.-Y., Song, M.-D., Kim, J.-W. and Baik, J.-J. 2001. Effects of gravity wave drag induced by cumulus convection on the atmospheric general circulation. *J. Atmos. Sci.* **58**, 302–319.

Edmon, H. J. Jr., Hoskins, B. J. and McIntyre, M. E. 1980. Eliassen–Palm cross-sections for the troposphere. *J. Atmos. Sci.* **37**, 2600–2616.

Egger, J. 2003. Gravity wave drag and global angular momentum: geostrophic adjustment processes. *Tellus* **55A**, 419–425.

Emanuel, K. A. and Zivkovic-Rothman, M. 1999. Development and evaluation of a convection scheme for use in climate models. *J. Atmos. Sci*. **56**, 1766–1782.

Goerss, J. S. and Phoebus, P. 1992. The Navy's operational atmospheric analysis. *Wea. Forecasting* **7**, 232–249.

Gregory, D., Shutts, G. J. and Mitchell, J. R. 1998. A new gravity-wave-drag scheme incorporating anisotropic orography and low-level wave breaking: impact upon the climate of the UK Meteorological Office Unified Model. *Q. J. R. Meteorol. Soc.* **124**, 463–493.

Harshvardhan, Davies, R., Randall, D. and Corsetti, T. 1987. A fast radiation parametrization for atmospheric circulation models. *J. Geophys. Res.* **92**, 1009–1016.

Haynes, P. H., Marks, C. J., McIntyre, M. E., Shepherd, T. G. and Shine, K. P. 1991. On the 'downward control' of extratropical diabatic circulations by eddy-induced mean zonal forces. *J. Atmos. Sci.* **48**, 651–678.

Hogan, T. and Rosmond, T. 1991. The description of the Navy Operational Global Atmospheric Prediction System's spectral forecast model. *Mon. Wea. Rev.* **119**, 1186–1815.

Hogan, T., Rosmond, T. and Gelaro, R. 1991. The NOGAPS forecast model: a technical description. NOARL Report 13, 220 pages.

Hogan, T. and Brody, L. 1993. Sensitivity Studies of the Navy's global forecast model parametrizations and evaluation of improvements to NOGAPS. *Mon. Wea. Rev.* **121**, 2373–2395.

Huang, H. P., Sardeshmukh, P. D. and Weickmann, K. M. 1999. The balance of global angular momentum in a long-term atmospheric data set. *J. Geophys. Res.* **104**, 2031–2040.

Kim, Y.-J. 1996. Representation of subgrid-scale orographic effects in a general circulation model: Part I. Impact on the dynamics of simulated January climate. *J. Climate* **9**, 2698–2717.

Kim, Y.-J. and Arakawa, A. 1995. Improvement of orographic gravity-wave parametrization using a mesoscale gravity-wave model. *J. Atmos. Sci.* **52**, 1875–1902.

Kim, Y.-J., Eckermann, S.D. and Chun, H.-Y. 2003. An overview of the past, present and future of gravity-wave drag parametrization for numerical climate and weather prediction models. *Atmosphere-Ocean* **41**, 65–98 (available on-line at http://www.cmos.ca/Ao/Papersfull/v410105.pdf).

Kim, Y.-J., Farrara, J. D. and Mechoso, C. R. 1998. Sensitivity of AGCM simulations to modifications in the ozone distribution and refinements in selected physical parametrizations. *J. Meteorol. Soc. Japan* **76**, 695–709.

Klinker, E. and Sardeshmukh, P. D. 1992. The diagnosis of mechanical dissipation in the atmosphere from large-scale balance requirements. *J. Atmos. Sci.* **49**, 608–627.

Kodera, K., Yamazaki, K., Chiba, M. and Shibata, K. 1990. Downward propagation of upper stratospheric mean zonal wind perturbation to the troposphere. *Geophy. Res. Lett.* **17**, 1263–1266.

Kuroda, Y. 2002. Relationship between the polar night jet oscillation and the annular mode. *Geophy. Res. Lett.* **29**, 81.

Lejenäs, H., Madden, R. A. and Hack, J. J. 1997. Global atmospheric angular momentum and Earth–atmosphere exchange of angular momentum simulated in a general circulation model. *J. Geophys. Res.* **102**, 1931–1941.

Lott, F. and Miller, M. J. 1997. A new subgrid-scale orographic parametrization: its formulation and testing. *Q. J. R. Meteorol. Soc.* **123**, 101–127.

Louis, J. F. 1979. A parametric model of vertical eddy fluxes in the atmosphere. *Boundary Layer Meteorol.* **17**, 187–202.

McFarlane, N. A. 1987. The effect of orographically excited gravity-wave drag on the general circulation of the lower stratosphere and troposphere. *J. Atmos. Sci.* **44**, 1775–1800.

Milton, S. F. and Wilson, C. A. 1996. The impact of parametrized subgrid-scale orographic forcing on systematic errors in global NWP model. *Mon. Wea. Rev*. **124**, 2023–2045.

Palmer, T. N., Shutts, G. J. and Swinbank, R. 1986. Alleviation of a systematic westerly bias in general circulation and numerical weather prediction models through an orographic gravity wave drag parametrization. *Q. J. R. Meteorol. Soc.* **112**, 1001–1039.

Peixoto, J. P. and Oort, A. H. 1992. *Physics of Climate*. American Institute of Physics, New York, 520 pp.

Robinson, W. A. 1986. The application of the quasi-geostrophic Eliassen–Palm flux to the analysis of stratospheric data. *J. Atmos. Sci.* **43**, 1017–1023.

Rontu, L. and Boutier, F. 2002. In: *HIRLAM Workshop on Mesoscale Modelling*, Dublin, 14–16 October (available at http://hirlam.knmi.nl).

Rontu, L., Sattler, K. and Sigg, R. 2002. Parametrization of subgrid-scale orography effects in HIRLAM. *HIRLAM Technical Report 56* (available at http://hirlam.knmi.nl).

Rosmond, T. E. 1992. The design and testing of the Navy operational global atmospheric prediction system. *Wea. Forecasting* **7**, 262–272.

Salstein, D. A., Kann, D. M., Miller, A. J. and Rosen, R. D. 1993. The sub-bureau for atmospheric angular momentum of the International Earth Rotation Service: a meteorological data center with geodetic applications. *Bull. Am. Meteorol. Soc.* **74**, 67–80.

Scinocca, J. F. and McFarlane, N. A. 2000. The parametrization of drag induced by stratified flow over anisotropic topography. *Q. J. R. Meteorol. Soc.* **126**, 2353–2393.

Shepherd, T. G., Semeniuk, K. and Koshyk, J. N. 1996. Sponge layer feedbacks in middle-atmosphere models. *J. Geophys. Res*. **101**, 23,447–23,464.

Slingo, J. M. 1987. The development and verification of a cloud prediction scheme in the ECMWF model. *Q. J. R. Meteorol. Soc.* **113**, 899–927.

Swinbank, R. 1985. The global atmospheric angular-momentum balance inferred from analyses made during the FGGE. *Q. J. R. Meteorol. Soc.* **111**, 977–992.

Teixeira, J. and Hogan, T. F. 2002. Boundary layer clouds in a global atmospheric model: simple cloud cover parametrizations. *J. Climate* **15**, 1261–1276.